Postprint of: Xu X., Zhu D., Wang X., Deng L., Fan X., Ding Z., Zhang A., Xue G., Liu Y., Xuan W., Li X., Mąkinia J., Transformation of polyvinyl chloride (PVC) into a versatile and efficient adsorbent of Cu(II) cations and Cr(VI) anions through hydrothermal treatment and sulfonation, JOURNAL OF HAZARDOUS MATERIALS, Vol. 432, Part A (2021), 126973, DOI: 10.1016/j.jhazmat.2021.126973

Transformation of polyvinyl chloride (PVC) into a versatile and efficient adsorbent of Cu(II) cations and Cr(VI) anions through hydrothermal treatment and sulfonation

Xianbao Xu[a], Daan Zhu[a], Xiaonuan Wang[a], Liling Deng[a], Xinyun Fan[d], Zizhen Ding[a], Ai Zhang[a], Gang Xue[a], Yanbiao Liu[a], Weimin Xuan[c], Xiang Li[a,] *, Jacek Makinia[b]

[a] *College of Environmental Science and Engineering, State Environmental Protection Engineering Centre for Pollution Treatment and Control in Textile Industry, Donghua University, 2999 North Renmin Road, Shanghai 201620, China*

[b] *Faculty of Civil and Environmental Engineering, Gdansk University of Technology, ul. Narutowicza 11/12, 80-233 Gdansk, Poland*

[c] *College of Chemistry, Chemical Engineering and Biotechnology, Donghua University, 2999 North Renmin Road, Shanghai 201620, China*

[d] *State Key Laboratory of Pollution Control and Resources Reuse, School of Environmental Science and Engineering, Tongji University, 1239 Siping Road, Shanghai 200092, China*

*Corresponding author

E-mail: lix@dhu.edu.cn

Tel: 86-21-67792538

Fax: 86-21-67792159

Abstract

The reuse of waste polyvinyl chloride (PVC) has drawn much attention as it can reduce plastic waste and associated pollution, and provide valuable raw materials and products. In this study, sulfonated PVC-derived hydrochar (HS-PVC) was synthesized by two-stage hydrothermal treatment (HT) and sulfonation, and shown to be a versatile adsorbent. The reoval of Cu(II) cations and Cr(VI) anions using HS-PVC reached 81.2 ± 1.6% and 60.3 ± 3.8%, respectively. The first stage of HT was crucial for the dichlorination of PVC and the formation of an aromatic structure. This stage guaranteed the introduction of -SO_3H onto PVC-derived hydrochar through subsequent sulfonation. HT intensities (i.e., temperature and time) and sulfonation intensity strongly determined the adsorption capacity of HS-PVC. Competitive adsorption between Cu(II) and Cr(VI) onto HS-PVC was demonstrated by binary and preloading adsorption. The proposed Cu(II) cations adsorption mechanism was electrostatic adsorption, while Cr(VI) were possibly complexed by the phenolic -OH and reduced to Cr(III) cations by C=C groups in HS-PVC. In addition, HS-PVC derived from PVC waste pipes performed better than PVC powder for Cu(II) and Cr(VI) removal (> 90%). This study provides an efficient method for recycling waste PVC and production of efficient adsorbents.

Keywords: Polyvinyl chloride; Hydrothermal treatment; Sulfonation; Adsorption; Cu(II) cations and Cr(VI) anions

1. Introduction

Polyvinyl chloride (PVC) is irreplaceable in the infrastructure of modern society (Cui et al., 2021). However, large quantities of plastic waste continuously enter aquatic and terrestrial ecosystems, leading to ubiquitous pollution worldwide (Kawecki and Nowack 2019, Miao et al., 2020). For example, the accumulated PVC waste in China will exceed 500 million tons by the end of 2050, posing a daunting challenge for the safe and effective disposal of this halogenated waste (Liu et al., 2020).

Mechanical recycling (25.5%), incineration (9.3%), and landfill disposal (36.0%) are currently the main solutions for solving the problem of PVC waste (Yu et al., 2016, Ye et al., 2017, Liu et al., 2020). However, mechanical recycling is still rudimentary and only suitable for source-separated PVC waste. Incineration and landfill disposal of PVC waste normally release hazardous compounds, such as polychlorinated dibenzo-p-dioxins and polychlorinated dibenzofurans. Furthermore, the land requirements of landfills must be considered (Wiedinmyer et al., 2014). Thus, reliable alternative methods to treat PVC waste safely and efficiently in an environmentally sound and high value-added way are worth pursuing (Lau et al., 2020). Such an approach is in line with the European Union's strategy for plastics in a circular economy (Matthews et al., 2021).

Hydrothermal treatment (HT), conducted at relatively low temperatures of 160 to 300°C, can pretreat PVC waste for dehydrochlorination (Ma et al., 2019, Ning et al., 2020), permitting subsequent pyrolysis to produce chars and liquid hydrocarbons with a low Cl content, such as alkene and polyene (Poerschmann et al., 2015, Jiang et al., 2021). However,

63 cost- and energy-intensive conditions, such as noble metal catalysts and high temperature
64 (500℃), are typically adopted for lighter oil production by catalytic pyrolysis of plastic
65 (Kunwar et al., 2016, Maity et al., 2020). On the other hand, PVC waste can be converted
66 into coal-alternative fuels by HT processes amended with cellulose (Shen et al., 2017),
67 pinewood sawdust (Huang et al., 2019), and corncob (Lu et al., 2020). Yet, another important
68 recycling method has been undervalued and ignored, i.e., the potential transformation of
69 PVC-derived hydrochar (H-PVC) into an effective adsorbent for the removal of contaminants,
70 such as heavy metals.

71 Unfortunately, the adsorption capacity of organic compounds by H-PVC is very low,
72 primarily because surface-related adsorption prevails over hydrophobic partitioning
73 (Poerschmann et al., 2015). Several studies showed that the adsorption of hydrochar derived
74 from natural biomass sources was enhanced by introducing functional groups, such as −OH,
75 −COOH, and $-NH_2$, which could trap heavy metal ions from aqueous solutions (Azzaz et al.,
76 2020, Yang et al., 2021). Sulfonation is an attractive modifications method for various carbon
77 materials due to the unique surface chemistry and low production costs. Large amounts of
78 oxygen functionalities, such as −OH, −COOH, and lactones, along with $-SO_3H$ groups, are
79 introduced into the surface of the carbon materials, improving their hydrophilic/oxyphilic
80 properties after sulfonation. Sulfonated carbon materials have been widely applied in the
81 catalysis of esterifications, acetalization, etherifications, and transesterifications (Konwar et
82 al., 2019). However, sulfonated PVC-derived hydrochar (HS-PVC) has rarely been reported,
83 albeit potentially being a cost-effective adsorbent for heavy metals.

The novelty of the present work is the development of two-stage HT and sulfonation to synthesize PVC-derived adsorbents for the removal of both Cu(II) cations and Cr(VI) anions. A systematic investigation was conducted to discern the mechanisms underlying functional group modifications of PVC through different strategies and treatment intensities. The adsorption mechanisms of Cu(II) and Cr(VI) were clarified to understand the adsorption behavior onto HS-PVC. The performance of HS-PVC to adsorb Cu(II) and Cr(VI) from natural water was evaluated. PVC waste pipes were used to synthesize HS-PVC and test its applications. Furthermore, the versatility of HS-PVC for the adsorption of low concentrations of Cu(II) and Cr(VI) (20 mg/L) and other metals, i.e., Mn(II), Cd(II), Ni(II), and Co(II) was investigated. This study provides a practical approach for the sustainable reuse of waste PVC as an efficient adsorbent to remove heavy metal cations and anions.

2. Materials and methods

2.1. Preparation of PVC-derived adsorbents

Raw PVC powder (sieved through a 100 mesh) was purchased from a plastic chemical company (Guangdong, China). Hydrothermal batch reactions were conducted by loading 10 g of Raw PVC with 40 mL distilled water in 100-mL airtight stainless-steel tubular reactors with internal polyphenylene containers. The reactors were heated to 250 ℃ for 6 h in a homothermic oven (DHG-9013A, China). The reactors were then cooled to room temperature in a water bath to prepare the H-PVC. Ten grams of Raw PVC was sulfonated in flasks (250 ml) with concentrated sulfuric acid (98%) at a sulfonation intensity of 1:10 (g/mL) in a shaking

bath (70 ℃ and 110 rpm for 12 h) to produce the sulfonated PVC (S-PVC). Unless otherwise specified, sulfonation intensity refers to the ratio of adsorbent mass to the volume of sulfuric acid in this paper. Specifically, a relatively low temperature of sulfonation (70 ℃) was chosen according to the literature (Xiao and Hill 2020). The HS-PVC was synthesized by sulfonation of H-PVC with the same process as described for S-PVC. The S-PVC and HS-PVC were washed three times with distilled water to eliminate the unreacted sulfuric acid. The Raw PVC, H-PVC, S-PVC, and HS-PVC were dried in a homothermic oven at 105 ℃ for 24 h. The dried PVC-derived adsorbents were then ground and sieved through a 100 mesh (147 um) before adsorption of Cu(II) and Cr(VI).

2.2. PVC-derived adsorbents for highly efficient removal of Cu(II) and Cr(VI)

2.2.1. Cu(II) and Cr(VI) removal using Raw PVC, H-PVC, S-PVC, and HS-PVC

A stock solution of 500 mg Cu(II)/L (7.87 mM) was prepared by dissolving 1965 mg of copper sulfate pentahydrate ($CuSO_4 \cdot 5H_2O$) in 1 L of ultrapure water. A stock solution of 250 mg Cr(VI)/L (4.81 mM) was prepared by dissolving 770 mg of potassium dichromate ($K_2Cr_2O_7$) in 1 L of ultrapure water. Batch experiments of Cu(II) and Cr(VI) removal were performed by adding 10 g/L of Raw PVC, H-PVC, S-PVC, and HS-PVC to flasks (250 mL) in a water bath shaker (25 ℃ and 100 rpm) for 12 h. All samples were withdrawn from the flasks and filtered through membrane filters with a pore size of 0.22 μm for subsequent Cu(II) and Cr(VI) determination.

The removal efficiencies of Cu(II) and Cr(VI) were calculated as:

$$\text{Removal efficiency} = \frac{C_0 - C_t}{C_0} \times 100\% \quad (1)$$

where C_0 (mg/L) and C_t (mg/L) were the concentrations of Cu(II) and Cr(VI) at the start of the experiment and time t (h). Unless otherwise specified, all calculations of Cu(II) and Cr(VI) removal efficiencies by PVC-derived adsorbents followed this equation. The concentrations of Cu(II) and Cr(VI) were determined by inductively coupled plasma mass spectrometry (ICP-MS) (Thermo Scientific iCAP Q, USA).

2.2.2. Cu(II) and Cr(VI) removal using HS-PVC under different intensities of HT temperature, HT time, and sulfonation and correlation analyses

HS-PVC was synthesized under different intensities of HT (temperature and time) and sulfonation as follows: HT temperatures from 220 ℃ to 260 ℃ (in 10 ℃ intervals, HT time of 6 h and sulfonation intensity of 1:10), HTC times from 2 h to 6 h (in 1 h intervals, HT temperature of 250 ℃, and sulfonation intensity of 1:10), and sulfonation intensities from 1:1 to 1:10 (in 1:10 intervals, HT temperature of 250 ℃, and HT time of 6 h). 10 g/L HS-PVC fabricated with different HT intensities and sulfonation were used for Cu(II) and Cr(VI) removal at 25 ℃ and 100 rpm. To investigate the individual effects of the intensities of HT temperature, HT time, and sulfonation on Cu(II) and Cr(VI) removal, enhancements of Cu(II) and Cr(VI) removal were calculated by comparing the lowest value with the highest one (250 ℃ vs. 220℃, 6 h vs. 2 h, and 1:10 vs. 1:1, respectively).

2.2.3. Adsorption kinetics and isotherms of Cu(II) and Cr(VI) removal using HS-PVC

The adsorption kinetics of Cu(II) and Cr(VI) removal were studied based on the removal efficiencies of HS-PVC as described in Section 2.2.1. Adsorption isotherm experiments were carried out with different initial concentrations of Cu(II) (i.e., 100, 200, 300, 400, 500, 600,

and 800 mg/L) and Cr(VI) (50, 100, 150, 200, 250, and 300 mg/L) at three different temperatures (25, 35, and 45 °C) using 10 g/L HS-PVC under optimum operational conditions (250°C, 6 h, and a sulfonation intensity of 1:10).

Pseudo-first-order (PFO) and pseudo-second-order (PSO) models were used to evaluate Cu(II) and Cr(VI) removal kinetics of HS-PVC, and their linearized equations are given in *Eqs.* (2) and (3), respectively.

$$\ln(q_e - q_t) = \ln q_e - k_1 \mathrm{t} \quad (2)$$

$$\frac{t}{q_t} = \frac{1}{k_2 q_e^2} + \frac{t}{q_e} \quad (3)$$

where k_1 and k_2 are the rate constants of PFO and PSO, respectively, and q_e and q_t (mg/g) are the amounts of adsorbed Cu(II) and Cr(VI) (mg/g) at equilibrium and at time *t*, respectively. Values of k_1, k_2, and q_e were calculated based on the Levenberg-Marquardt method at the 95% confidence level.

To predict the adsorption capacity of the adsorbents, two widely used isotherms (i.e., Langmuir and Freundlich) were selected among several models. *Eqs*. (4) and (5) express the Langmuir isotherm and the Freundlich isotherm, respectively.

$$q_e = \frac{b q_m C_e}{1 + b C_e} \quad (4)$$

$$q_e = K_F C_e^{1/n} \quad (5)$$

where q_m (mg/g) is the maximum adsorption capacity of the adsorbent and *b* (L/mg) is the Langmuir constant related to the adsorption energy. K_F (mg/g) is the Freundlich adsorption isotherm constant related to the extent of adsorption and *n* is the heterogeneity factor of the Freundlich model. Values of *b*, q_m, K_F, and *n* were also calculated based on the

168 Levenberg-Marquardt method at the 95% confidence level.

169 **2.2.4. Competitive adsorption of Cu(II) and Cr(VI) onto HS-PVC in binary solution and**

170 **preloading adsorption**

171 Binary adsorption of Cu(II) and Cr(VI) was carried out by adding 10 g/L of HS-PVC to

172 a binary solution with 500 mg Cu(II)/L and 250 mg Cr(VI)/L in the same solution to

173 investigate the competitive adsorption between Cu(II) and Cr(VI). A separation factor was

174 utilized to investigate the adsorption selectivity in the binary solution, defined as:

175 $$\alpha_2^1 = \frac{q_{e1} \times C_{e2}}{C_{e1} \times q_{e2}} \quad (6)$$

176 where q_{e1} (mmol/g) and C_{e1} (mmol/L) were the equilibrium adsorption capacity and

177 equilibrium concentration toward constituent 1, and q_{e2} (mmol/g) and C_{e2} (mmol/L) were the

178 equilibrium adsorption capacity and equilibrium concentration toward constituent 2,

179 respectively.

180 Preloading adsorption tests for Cr(VI) were performed by incubating 2.5 g HS-PVC in

181 250 mg/L Cr(VI) solution for 12 h. Then, the HS-PVC preloaded with Cr(VI) was used for

182 the adsorption of Cu(II) for 12 h, as described in Section 2.2.1. The preloading adsorption

183 tests for Cu(II) were performed under the same experimental conditions as those for Cr(VI).

184 The removal efficiencies of Cu(II) and Cr(VI) were calculated to evaluate the competitive

185 adsorption between Cu(II) and Cr(VI) onto the HS-PVC.

186 **2.2.5. Effect of K(I) on Cr(VI) removal**

187 The cations K(I) was present in the experimental Cr(VI) solutions prepared from

188 $K_2Cr_2O_7$. To assess the impact of K(I) on the adsorption of Cr(VI) by HS-PVC, $HClO_4$ (36.62

mL, calculated as described in Text S1) was added to precipitate K(I) (*Ksp* of $KClO_4$ 1.5×10^{-2}) in the Cr(VI) solution (total volume 100 mL). Then, HS-PVC (10 g/L) was added to the treated Cr(VI) solution for adsorption for 12 h. Finally, the removal efficiency of Cr(VI) was calculated to evaluate the impact of K(I) on the adsorption of Cr(VI) using HS-PVC.

2.2.6. Low concentration Cu(II) and Cr(VI) removal using HS-PVC

The concentrations of Cu(II) and Cr(VI) in industrial applications, such as electroplating, leather tanning, and alloy manufacturing, range from 20 to 600 mg/L. Thus, 10 g/L of HS-PVC was added to 20 mg/L Cu(II) and Cr(VI) solutions to evaluate its adsorption performance for low concentrations of these heavy metals. The adsorption procedure was the same as in Section 2.2.1.

2.2.7. Cu(II) and Cr(VI) removal in natural water

To test the potential interference of natural water regarding Cu(II) and Cr(VI) adsorption on HS-PVC, natural water (untreated surface water) was sampled from the Jingyue Lake in Donghua University, Shanghai, China. This water was used to prepare Cu(II) (500 mg/L) and Cr(VI) (250 mg/L) solutions. 10 g/L of HS-PVC was added to these Cu(II) and Cr(VI) solutions and incubated for 12 h at 25℃ and 100 rpm.

2.2.8. Cu(II) and Cr(VI) removal using HS-PVC derived from PVC waste pipes

To test the applications of HS-PVC in Cu(II) and Cr(VI) removal, real PVC waste pipes were used to prepare HS-PVC (real waste PVC). First, the PVC waste pipes were fragmented with a crusher and then washed with tap water. Subsequently, 10 g/L of the pretreated HS-PVC from pipes was added to Cu(II) (500 mg/L) and Cr(VI) (250 mg/L) solutions for 12

h adsorption (at 25℃ and 100 rpm).

2.3. Characterizations of PVC-derived adsorbents

2.3.1. Characterizations of Raw PVC, H-PVC, S-PVC, and HS-PVC

The surface properties of Raw PVC, H-PVC, S-PVC, and HS-PVC were characterized by scanning electron microscopy (SEM) (HITACHI, S-4800, Japan) and contact angle measurements (θ) (Kino, SL200KS, USA). The specific surface area and pore distribution of Raw PVC, H-PVC, S-PVC, and HS-PVC were determined by the Brunauer−Emmett−Teller (BET) (Quantachrome, Autosorb-iQ, USA) method and mercury intrusion porosimetry (MIP) (Micromeritics, Auto pore lv, USA), respectively. Particle size distributions were calculated based on the SEM images (Table S1). The elemental composition of Raw PVC, H-PVC, S-PVC, and HS-PVC was analyzed by elemental analysis (Elementar, EL III, Germany) and energy dispersive spectroscopic (EDS) (IE 300 X, England) element mapping. The variation of functional groups of Raw PVC, H-PVC, S-PVC, and HS-PVC was characterized by Fourier transform infrared (FTIR) spectroscopy (Thermo Fisher, NEX US-670, USA). The thermostability of Raw PVC and HS-PVC was evaluated by thermogravimetric analysis (TGA, TA, Netzsch, Germany).

2.3.2. Characterizations of HS-PVC before and after adsorption of Cu(II) and Cr(VI)

The electric potentials of HS-PVC, HS-PVC after adsorption of Cu(II) (HS-PVC-Cu), and HS-PVC after adsorption of Cr(VI) (HS-PVC-Cr) were determined by zeta potential measurements (Brook Haven, 90 PALS, USA). In addition, the functional groups of HS-PVC and HS-PVC-Cr were analyzed by X-ray photoelectron spectroscopy (XPS) (Thermo

231 Scientific, K-Alpha, USA), FTIR, solid-state ^{13}C nuclear magnetic resonance spectroscopy
232 (NMR) (Agilent, 600M, USA), and Raman spectroscopy (Thermo Fisher, DXR, USA). The
233 C1s XPS spectra were separated and characterized by C=C (284.8 eV), C-C (285.1 eV), C-O
234 (286.1 eV), and C=O groups (288.7 eV). The regions of functional groups derived from the
235 solid-state ^{13}C NMR spectra were divided into Carboxylic (220-161), Aromatic (161-113),
236 Anomeric (113-93), Carbohydrate (93-44), and Alkyl (44-0) (Wang et al., 2016, Li et al.,
237 2019).

238 **2.4. Statistical analysis**

239 All adsorption experiments were run in triplicate, and the results were expressed as
240 mean values ± standard deviation. The triplicate PVC-derived adsorbents were pooled to
241 minimize the potential variation before its characterizations (SEM, MIP, elemental analysis,
242 FTIR, TGA, XPS, solid-state ^{13}C NMR, and Raman spectroscopy). Analyses of variance
243 (ANOVA) were used to test for differences between treatments, and $p<0.05$ was considered
244 statistically significant.

245

246 **3. Results and discussion**

247 **3.1. Highly efficient Cu(II) cations and Cr(VI) anions removal using HS-PVC**

248 Regarding Cu(II) removal, HS-PVC was significantly more efficient (81.2 ± 1.6%)
249 compared to Raw PVC (28.5 ± 1.7%) and PVC solely pretreated by either HT (14.5 ± 3.2%)
250 or sulfonation (20.6 ± 4.8%) within 12 h (Fig. 1A). In addition, HS-PVC was also highly
251 efficient in removing Cr(VI) (60.3 ± 3.8%) compared to Raw PVC (6.1 ± 1.3%) and PVC

252 solely pretreated by either HT (14.0 ± 4.6%) or sulfonation (7.0 ± 4.8%) within 12 h (Fig.
253 1B). The adsorption of Cu(II) reached equilibrium within 30 min while the adsorption
254 efficiency of Cr(VI) was only 49.3 ± 1.0% at 30 min and then slowly increased to equilibrium
255 within 3 h (Fig. S1). This suggested different adsorption mechanisms for Cu(II) and Cr(VI)
256 onto HS-PVC. Biomass-derived hydrochar was also widely employed in the adsorption of
257 metal cations, such as Cu(II), Zn(II), and Pb(II) (Deng et al., 2020, Kazak and Tor 2020, Song
258 et al., 2020) or metal anions, such as Cr(VI) ($Cr_2O_7^{2-}$) (Li et al., 2020). Cu(II) and Cr(VI)
259 could be simultaneously removed by hydrochar derived from chitosan with Fe_2O_3
260 modifications. However, the main adsorption mechanisms were chelation adsorption of Cu(II)
261 and electrostatic adsorption-coupled Cr(VI) reduction due to the specific dual-core Fe_2O_3@C
262 structure (Wang et al., 2017). The present study firstly provided a metal-free modification of
263 hydrochar derived from waste PVC for simultaneous Cu(II) cations and Cr(VI) anions
264 removal.

265 The adsorption capacity of hydrochar was highly dependent on the functional groups
266 formed during HT (Tong et al., 2021). However, the structure and component of PVC
267 ([-CH_2-CHCl-]n) were simpler compared to natural biomass, suggesting fewer functional
268 groups anchored in H-PVC than in natural biomass. This may explain why H-PVC is of little
269 significance for the adsorption of Cu(II) and Cr(VI) (Fig. 1), which was in line with poor
270 adsorption in wastewater remediation (Poerschmann et al., 2015). Sulfonation was also an
271 efficient modification of adsorbents derived from tea waste and cellulose for Cu(II) or Cr(VI)
272 removal (Dong et al., 2016, Ahsan et al., 2018). However, the adsorption of Cu(II) and Cr(VI)

using S-PVC was still low in this study. This paper showed a possible synergistic effect of HT and sulfonation in the modifications of the methodology to produce a highly efficient adsorbent.

3.2. Characterization during the fabrications of HS-PVC from Raw PVC in combination with HT and sulfonation

The microstructure of the PVC-derived adsorbents was characterized by SEM (Fig. 2A to 2D). A rough surface and non-porous structures were observed in Raw PVC (Fig. 2A). After HT treatment, the surface of H-PVC became smoother with an internal porous structure (Fig. 2B) mainly due to dehydrochlorination, aromatization, and depolymerization reactions during HT (Ning et al., 2020). There was no apparent difference between Raw PVC and S-PVC in the SEM images (Fig. 2A and 2C), indicating that sulfonation possessed a marginal impact on the surface structure. In contrast, the HS-PVC was fragmented with an internal porous structure due to HT and sulfonation (Fig. 2D), which was consistent with a significant decrease of particle size in HS-PVC compared to the Raw PVC (Fig. 3A and Table S2). In addition, the hydrophobicity and hydrophilicity of adsorbents may influence the performance of the adsorption process (Adam et al., 2020). The hydrophobicity of S-PVC was similar to that of Raw PVC (Fig. 2E and 2G). However, the hydrophobicity was higher after HT (Fig. 2E and 2F), resulting in hydrophobic partitioning as described in the literature (Poerschmann et al., 2015), which was consistent with the low adsorption efficiency of Cu(II) and Cr(VI) by H-PVC (Fig. 1). Furthermore, the hydrophilicity of HS-PVC was significantly higher than that of H-PVC (Fig. 2F and 2H), indicating that sulfonation improved the hydrophilicity of

HS-PVC, which is a prerequisite for the adsorption of Cu(II) and Cr(VI).

The BET surface areas of Raw PVC (2.59 m^2/g), H-PVC (4.95 m^2/g), S-PVC (2.01 m^2/g), and HS-PVC (0.59 m^2/g) (Table S3) were relatively low compared to those of biomass-derived hydrochar (118 m^2/g) in the literature (Sheng et al., 2019). According to the analysis of MIP (Fig. S2), the pore size in HS-PVC was mainly in the mesoporous (2-50 nm) and microporous (>50 nm) regions (Erdem et al., 2020, Rueda-Marquez et al., 2021). The results revealed that the Cu(II) and Cr(VI) adsorption mostly occurred in the mesoporous and microporous regions of the HS-PVC.

Elemental analysis (Fig. 3B) showed that the Cl/C molar ratio (0.5) of Raw PVC was similar to the stoichiometric value of ($[-CH_2-CHCl-]_n$). However, the molar ratio of Cl/C on the surface of Raw PVC (0.85 ± 0.37) was higher than 0.5 according to EDS element mapping (Fig. 3C), suggesting that most of the -Cl functional groups were on the surface of Raw PVC. The Cl/C ratio of H-PVC significantly decreased (Fig. 3B and 3C) compared to the Raw PVC after pretreatment by HT due to the dehydrochlorination (Poerschmann et al., 2015). The elemental composition of the entire Raw PVC and S-PVC was similar (Fig. 3B), but surface Cl was lower, and surface O slightly higher in S-PVC than in Raw PVC (Fig. 3C). This indicated that sole sulfonation only impacted the chemical composition on the surface of Raw PVC (Fig. 3C), causing no obvious chemical modifications to the entire Raw PVC (Fig. 3B). Additionally, the O/C and S/C ratios of HS-PVC increased, resulting in an O/S ratio of 3.04 (elemental analysis in Fig. 3B) or 3.16 (EDS element mapping in Fig. 3C). Thus, it could be hypothesized that the introduction of S-containing functional groups such as $-SO_3H$

315 (O/S=3) into HS-PVC occurred. The absorption peaks of HS-PVC from the FTIR at 1030
316 cm^{-1} (O=S=O) and 1169 cm^{-1} (-SO_3H) verified this assumption (Fig. 3D) (Chen et al., 2019).
317 The functional group -SO_3H was only detected in HS-PVC, indicating that the introduction of
318 -SO_3H onto HS-PVC was attributed to the synergy effect of HT and sulfonation. In addition,
319 the thermostability of HS-PVC was higher than that of Raw PVC according to the TGA
320 patterns (Fig. S3), which was mainly due to aromatization during HT (Park et al., 2016). It
321 has been reported that the presence of aromatic groups was essential for the sulfonation of
322 petroleum coke by concentrated H_2SO_4 (Xiao and Hill 2020). In this study, HT was crucial to
323 forming an aromatic structure (Fig. 3D) for the introduction of -SO_3H during sulfonation to
324 fabricate HS-PVC for highly efficient Cu(II) and Cr(VI) removal. Moreover, the functional
325 group C=C in HS-PVC (Fig. 3D) was crucial for removing Cr(VI), which was confirmed in
326 the following section.

327 **3.3. Correlations of Cu(II) and Cr(VI) removal with HT intensities and sulfonation**

328 The adsorption properties of HS-PVC were highly dependent on HT temperature and
329 time (see time curves in Fig. S4 and Fig. S5). The adsorption efficiencies of Cu(II) and Cr(VI)
330 increased from 36.9 ± 3.0% and 46.0 ± 3.8% at 220 ℃ to 81.1 ± 2.1% and 61.7 ± 2.7% at
331 250 ℃, but declined to 63.7 ± 3.2% and 57.2 ± 1.3% at 260 ℃, respectively (Fig. 4A). In
332 addition, the adsorption efficiencies of Cu(II) and Cr(VI) also increased from 56.5 ± 1.7%
333 and 9.2 ± 1.1% at 2 h to 80.0 ± 2.8% and 58.5 ± 1.1% at 6 h, followed by declines to 54.5 ±
334 2.0% and 2.2 ± 1.2% at 8 h, respectively (Fig. 4B). Higher HT intensities benefited PVC
335 dehydrochlorination (Zhang et al., 2020), providing more sites for subsequent SO_3H

introduction during sulfonation. It has been reported that proper HT intensities (HT temperature = 250 ℃ and HT time = 6 h in this study) benefited the formation of the aromatic structure (Ning et al., 2020). In contrast, higher HT intensities affected the stability of the carbon structure (Ning et al., 2020), which explained the declines in the adsorptions of Cu(II) and Cr(VI) onto HS-PVC at 260 ℃ (Fig. 4A) and 8 h (Fig. 4B).

The sulfonation intensity also affected the introduction of functional groups (Konwar et al., 2019), thus affecting the adsorptive performance of HS-PVC. The adsorption time curves of sulfonation intensity regarding Cu(II) and Cr(VI) removal by HS-PVC were shown in Fig. S6. With the increasing sulfonation intensity, the adsorption efficiencies of Cu(II) and Cr(VI) increased from 38.1 ± 3.2% and 28.4 ± 3.5% at the sulfonation intensity of 1:1 to 81.0 ± 1.3% and 59.6 ± 2.4% at the sulfonation intensity of 1:10 (Fig. 4C). The adsorption of Cu(II) and Cr(VI) was positively correlated with the increase in sulfonation intensity from 1:1 to 1:10.

As summarized in Fig. 4D, the adsorption efficiency of Cu(II) increased by 117.4% while that of Cr(VI) only by 34.1%, when increasing the temperature from 220 ℃ to 250 ℃. In contrast, the adsorption efficiency of Cu(II) improved only by 41.6%, while that of Cr(VI) increased by 534%, with HT time increasing from 2 to 8 h. These results indicated that the adsorption of Cu(II) was sensitive to HT temperature while the adsorption of Cr(VI) was rather sensitive to HT time. However, the impact of sulfonation intensity on the adsorption of Cu(II) (increasing 112.5% from 1:1 to 1:10) was similar to the adsorption of Cr(VI) (increasing 110.3% from 1:1 to 1:10).

3.4. Kinetics and isotherms of the adsorption of Cu(II) and Cr(VI) onto HS-PVC

Adsorption kinetics were essential to investigate the adsorption process (Song et al., 2020, Wang and Guo 2020). The adsorption of Cu(II) and Cr(VI) onto the HS-PVC (Fig. 5A and 5B) increased rapidly in the first 30 min and then decreased as the reaction approached equilibrium due to the saturation of active adsorbent sites. The values of q_e and rate constants (k_1 and k_2) obtained from the kinetic models (Fig. 5A and 5B) were shown in Table 1, along with the correlation coefficients (R^2). The R^2 value of the PSO model was higher than that of the PFO model for both Cu(II) and Cr(VI) adsorption. In addition, the q_e calculated by the PSO model was more consistent with the experimental value compared to that of the PFO model (Table 1). Hence, the adsorption process of Cu(II) and Cr(VI) onto HS-PVC could be well described by the PSO model, indicating that chemisorption might be the rate-limiting step. In addition, more active sites were reported with the PSO model compared to the PFO model (Wang and Guo 2020), which was crucial to the adsorption of Cu(II) and Cr(VI) onto HS-PVC.

Adsorption isotherms play a crucial role in investigating the chemical interactions between adsorbates and adsorbents (Yang et al., 2019, Wang and Guo 2020). The adsorption isotherms of the adsorption of Cu(II) and Cr(VI) onto HS-PVC at three different temperatures (25, 35, and 45℃) were shown in Fig. 5C-5F. During the adsorption of Cu(II), the R^2 values of the Langmuir model (0.94–0.96) were higher than those of the Freundlich model (0.82–0.89) at all tested temperatures (25, 35, and 45 ℃) (Fig. 5C, 5D, and Table S4), indicating that the adsorption of Cu(II) by HS-PVC was a monolayer process. Similarly, the adsorption

of Cr(VI) was also a monolayer process due to the higher R^2 values of the Langmuir model (0.94 at 25 ℃ and 0.95 at 35 ℃) compared to those of the Freundlich model (0.90 at 25 ℃ and 0.89 at 35 ℃) (Fig. 5E, 5F, and Table S4). However, the adsorption of Cr(VI) was fitted by the Langmuir and Freundlich model equally well according to R^2 values of 0.96 at 45℃. In addition, the values of K_F and q_m increased with the increasing temperature (Table S4), indicating an endothermic adsorption process (Xu et al., 2019).

3.5. Mechanisms for the adsorption of Cu(II) and Cr(VI) onto HS-PVC

The removal efficiency of Cu(II) decreased (p<0.01) by 19.9 % with the co-adsorption of Cr(VI), and that of Cr(VI) also significantly decreased (p<0.01) by 48.8% with the co-adsorption of Cu(II) (Fig. 6A). The selectivity of Cu(II) ($\alpha_{Cr(VI)}^{Cu(II)}$= 4.11) was higher than that of Cr(VI) ($\alpha_{Cr(VI)}^{Cu(II)}$= 0.24) in binary-component solution, indicating that Cu(II) can occupy adsorption sites more easily than Cr(VI). However, during the preloading test, the removal efficiency of Cu(II) decreased by 70.5% using Cr(VI) loaded HS-PVC, which was similar to the decrease in Cr(VI) removal (65.8%) using Cu(II) loaded HS-PVC (Fig. 6A). These results suggested that the Cu(II) and Cr(VI) adsorption might share similar adsorption sites on HS-PVC. The zeta potential, an important index for the electric potential at the mineral surface (Ramasamy et al., 2017, Gu et al., 2021), significantly decreased after HT and sulfonation (Fig. S7). The value increased after the adsorption of Cu(II) (Fig. 6B), indicating electrostatic adsorption (Fig. 7). However, only a slight increase in zeta potential was observed after the Cr(VI) adsorption, implying that other mechanisms govern Cr(VI) adsorption onto HS-PVC.

To further explore the mechanism of the adsorption of Cr(VI) onto HS-PVC, XPS analysis was used to investigate the adsorption behavior of hydrochar. The C1s XPS spectra were separated, and the characteristic C=C, C-C, C-O, and C=O bonds were quantified in HS-PVC before and after Cr(VI) adsorption. The intensity of C=C in HS-PVC decreased from 35.5% (Fig. 6C) to 28.5% (Fig. 6D) after adsorption of Cr(VI) (Fig. 6C), suggesting the involvement of this bond in Cr(VI) removal. According to solid-state ^{13}C NMR, aromatic functional groups decreased from 55.0% (Fig. 6 E) to 51.4% (Fig. 6F) after Cr(VI) adsorption, also supporting a decrease of C=C intensity after the adsorption of Cr(VI). In addition, the degree of graphitization of HS-PVC decreased after Cr(VI) adsorption according to the decrease in the ratio of I_G/I_D from 0.77 to 0.73 (Fig. 6G), which might be related to the reduction of Cr(VI). Interestingly, Cr(III) was detected in HS-PVC after the adsorption of Cr(VI) (Fig. 6H). These results indicated that the functional group C=C and aromatic groups might reduce Cr(VI) to Cr(III). In addition, there were shifts of the ring vibration peak in the FTIR spectra after adsorption of Cr(VI) (arrows in Fig. 6I). Since a ligand aligns itself to a metal, the energy of the ligand material will most likely be perturbed, leading ultimately to subtle shifts in the absorption peaks (Sergios et al., 2010). Thus, HS-PVC might also bind Cr(VI), which was consistent with Cr(III) and Cr(VI) in Fig. 6H. It has been reported that Cr(VI) was complexed with phenolic -OH using hydrochar derived from leaves and wood sticks. The adsorbed Cr(VI) was subsequently reduced to Cr(III) by the hydrochar along with the decrease of the functional group C=C (Chen et al., 2017, Chen et al., 2021). In this study, the Cr(VI) was supposed to be complexed by the phenolic -OH (Fig. 6I) existed in HS-PVC

and reduced by the C=C in the aromatic structure formed by HT (Fig. 7).

Note that the removal efficiency of Cr(VI) significantly decreased from 63.8 ± 2.0% in the presence of K(I) to 28.2 ± 5.1% after K(I) was precipitated by $HClO_4$ (Fig. S8). The introduction of H^+ ions increased the proportion of H_2CrO_4, thereby breaking the equilibrium balance of $HCrO_4^-$ and $Cr_2O_7^{2-}$ due to negative charges. This, in turn, suggested that K(I) ions might neutralize the negatively charged HS-PVC surface, thereby facilitating the binding of dichromate ions on HS-PVC (Fig. 7).

3.6. Versatility of HS-PVC

Natural water contains ions and organic compounds (Jeon et al., 2020), which might hinder Cu(II) and Cr(VI) removal by HS-PVC. Due to the competitive adsorption of co-existing ions, the efficient removal of Cu(II) and Cr(VI) decreased only by 19.2% and 25.0% (Fig. 8), respectively, indicating low interference. In addition, HS-PVC was particularly suitable for the removal efficiencies of Cu(II) and Cr(VI) at low concentrations (20 mg/L) (99.6 ± 0.1% and 94.3 ± 2.5%, respectively) (Fig. 8). Further, the removal efficiencies of Cu(II) and Cr(VI) using HS-PVC from waste pipes increased by 13.7% and 43.9% (Fig. 8), which were higher than those of HS-PVC derived from PVC powder (Fig. 1). The better performance of HS-PVC (pipes) might be attributed to plasticizers and mineral fillers in the PVC (Correa et al., 2019). The removal efficiencies of other metals such as Mn(II), Cd(II), Ni(II), and Co(II) amounted to 81.2 ± 2.3%, 80.8 ± 1.7%, 70.8 ± 1.8%, and 70.1 ± 3.2% (Fig. S9), respectively, indicating that HS-PVC is suitable for the treatment of complex industrial wastewater. Moreover, the adsorption of Cu(II) and Cr(VI) decreased only by 10.0% and 31.0% (Fig. S10)

after three adsorption-desorption cycles (1 mol/L HCl as eluent), indicating excellent recyclability.

Previous studies commonly focused on the conversion of waste PVC into coal-alternative fuel (Lu et al., 2020) or lighter oil (Maity et al., 2020). Using HT and sulfonation modifications, the present study provided a novel strategy for resource recovery of PVC waste by producing efficient adsorbents for Cu(II) cations and Cr(VI) anions removal. The sulfonation intensity was mild in this study (98% sulfuric acid at 70°C). Fuming H_2SO_4, $ClSO_3H$, aryldiazonium sulfonates, and higher temperatures (80–150°C) could be considered for additional optimization. In addition, as it is a "sulfonated carbon" (Konwar et al., 2019), HS-PVC may show promising catalytic performances in various organic transformations, including esterifications, ester exchange (transesterifications), acetalization, etherifications, condensation, and multi-component organic reactions that should be studied in the future.

4. Conclusion

This study provided a novel method to fabricate efficient adsorbent (HS-PVC) from waste PVC for both Cu(II) cations and Cr(VI) anions removal. The removal efficiencies of Cu(II) and Cr(VI) using HS-PVC reached 81.2 ± 1.6% and 60.3 ± 3.8%, respectively. The first stage of HT was crucial for the dichlorination of PVC and the formation of an aromatic structure, guaranteeing the introduction of $-SO_3H$ onto PVC-derived hydrochar through subsequent sulfonation. In addition, sulfonation also significantly increased the hydrophilicity of HS-PVC. The adsorption of Cu(II) was sensitive to HT temperature, while that of Cr(VI) was more sensitive to HT time. Adsorption isotherm data were accurately fitted by the

Langmuir isotherm model with a maximum adsorption capacity of 48.9 mg/g for the adsorption of Cu(II) and 20.2 mg/g for the adsorption of Cr(VI) at 45℃. Competitive adsorption of Cu(II) and Cr(VI) occurred, and the selectivity of HS-PVC for the removal of Cu(II) was higher than that of Cr(VI). The adsorption mechanism of Cu(II) was electrostatic adsorption, while Cr(VI) were possibly complexed by the phenolic -OH and reduced to Cr(III) cations by C=C groups in HS-PVC. In addition, HS-PVC was particularly suitable for the adsorption of both metals at low concentrations (＞94% at 20 mg/L). HS-PVC derived from PVC waste pipes also showed high absorption efficiencies for Cu(II) and Cr(VI) (＞90%).

Acknowledgments：

The authors acknowledge the financial support from the National Natural Science Foundation of China (NSFC) (51878137), National Key R&D Program of China (2019YFD1100502), Shanghai Rising-Star Program (20QA1400400), Shanghai Chen-Guang Program (19CG38).

References

Adam, M.C., Oscar, M.R.-N., Ayomi, J., Gehan De, S., Mahinda, I.R., Ashantha, G., Erick, R.B., 2020, Influence of surface hydrophobicity/hydrophilicity of biochar on the removal of emerging contaminants. Chem. Eng. J. http://dx.doi.org/10.1016/j.cej.2020.126277.

Ahsan, M.A., Katla, S.K., Islam, M.T., Hernandez-Viezcas, J.A., Martinez, L.M., Diaz-Moreno, C.A., Lopez, J., Singamaneni, S.R., Banuelos, J., Gardea-Torresdey, J., Noveron, J.C., 2018, Adsorptive removal of methylene blue, tetracycline and Cr(VI) from water using sulfonated tea waste. Environmental Technology & Innovation 11, 23-40. http://dx.doi.org/10.1016/j.eti.2018.04.003.

Azzaz, A.A., Khiari, B., Jellali, S., Ghimbeu, C.E.M., Jeguirim, M., 2020, Hydrochars production, characterization and application for wastewater treatment: A review. Renew. Sust.

Energ. Rev 127, 109882. http://dx.doi.org/10.1016/j.rser.2020.109882.

Chen, G., Wang, X., Jiang, Y., Mu, X., Liu, H., 2019, Insights into deactivation mechanism of sulfonated carbonaceous solid acids probed by cellulose hydrolysis. Catalysis Today 319, 25-30. http://dx.doi.org/10.1016/j.cattod.2018.03.069.

Chen, N., Cao, S., Zhang, L., Peng, X., Wang, X., Ai, Z., Zhang, L., 2021, Structural dependent Cr(VI) adsorption and reduction of biochar: hydrochar versus pyrochar. Sci. Total. Environ. 783. http://dx.doi.org/10.1016/j.scitotenv.2021.147084.

Chen, N., Huang, Y., Hou, X., Ai, Z., Zhang, L., 2017, Photochemistry of Hydrochar: Reactive Oxygen Species Generation and Sulfadimidine Degradation. Environ. Sci. Technol. 51(19), 11278-11287. http://dx.doi.org/10.1021/acs.est.7b02740.

Correa, C.A., de Santi, C.R., Leclerc, A., 2019, Green-PVC with full recycled industrial waste and renewably sourced content. Journal of Cleaner Production 229, 1397-1411. http://dx.doi.org/10.1016/j.jclepro.2019.04.383.

Cui, X., Zhang, J., Pan, M., Lin, Q., Khan, M.B., Yang, X., He, Z., Yan, B., Chen, G., 2021, Double-edged effects of polyvinyl chloride addition on heavy metal separation and biochar production during pyrolysis of Cd/Zn hyperaccumulator. Journal of Hazardous Materials. http://dx.doi.org/10.1016/j.jhazmat.2021.125793.

Deng, J., Li, X., Wei, X., Liu, Y., Liang, J., Song, B., Shao, Y., Huang, W., 2020, Hybrid silicate-hydrochar composite for highly efficient removal of heavy metal and antibiotics: coadsorption and mechanism. Chem. Eng. J. http://dx.doi.org/10.1016/j.cej.2020.124097.

Dong, C., Zhang, F., Pang, Z., Yang, G., 2016, Efficient and selective adsorption of multi-metal ions using sulfonated cellulose as adsorbent. Carbohyd. Polym. 151, 230-236. http://dx.doi.org/10.1016/j.carbpol.2016.05.066.

Erdem, C.U., Ateia, M., Liu, C., Karan, T., 2020, Activated carbon and organic matter characteristics impact the adsorption of DBP precursors when chlorine is added prior to GAC contactors. Water Res. 184, 116146. http://dx.doi.org/10.1016/j.watres.2020.116146.

Gu, S., Boase, E.M., Lan, C.Q., 2021, Enhanced Pb(II) removal by green alga Neochloris oleoabundans cultivated in high dissolved inorganic carbon cultures. Chem. Eng. J. 416. http://dx.doi.org/10.1016/j.cej.2021.128983.

Huang, N., Zhao, P., Ghosh, S., Fedyukhin, A., 2019, Co-hydrothermal carbonization of polyvinyl chloride and moist biomass to remove chlorine and inorganics for clean fuel production. Appl. Energ. 240, 882-892. http://dx.doi.org/10.1016/j.apenergy.2019.02.050.

Jeon, C., Solis, K.L., An, H.-R., Hong, Y., Igalavithana, A.D., Ok, Y.S., 2020, Sustainable removal of Hg(II) by sulfur-modified pine-needle biochar. Journal of Hazardous Materials 388. http://dx.doi.org/10.1016/j.jhazmat.2020.122048.

Jiang, G., Monsalve, D.A.S., Clough, P., Jiang, Y., Leeke, G.A., 2021, Understanding the Dechlorination of Chlorinated Hydrocarbons in the Pyrolysis of Mixed Plastics. Acs Sustain. Chem. Eng. 9(4), 1576-1589. http://dx.doi.org/10.1021/acssuschemeng.0c06461.

Kawecki, D., Nowack, B., 2019, Polymer-Specific Modeling of the Environmental Emissions of Seven Commodity Plastics As Macro- and Microplastics. Environ. Sci. Technol. 53(16), 9664-9676. http://dx.doi.org/10.1021/acs.est.9b02900.

Kazak, O., Tor, A., 2020, In situ preparation of magnetic hydrochar by co-hydrothermal

treatment of waste vinasse with red mud and its adsorption property for Pb(II) in aqueous solution. Journal of Hazardous Materials 393. http://dx.doi.org/10.1016/j.jhazmat.2020.122391.

Konwar, L.J., Maki-Arvela, P., Mikkola, J.-P., 2019, SO3H-Containing Functional Carbon Materials: Synthesis, Structure, and Acid Catalysis. Chem. Rev. 119(22), 11576-11630. http://dx.doi.org/10.1021/acs.chemrev.9b00199.

Kunwar, B., Cheng, H.N., Chandrashekaran, S.R., Sharma, B.K., 2016, Plastics to fuel: a review. Renew. Sust. Energ. Rev 54, 421-428. http://dx.doi.org/10.1016/j.rser.2015.10.015.

Lau, W.W.Y., Shiran, Y., Bailey, R.M., Cook, E., Stuchtey, M.R., Koskella, J., Velis, C.A., Godfrey, L., Boucher, J., Murphy, M.B., Thompson, R.C., Jankowska, E., Castillo, A.C., Pilditch, T.D., Dixon, B., Koerselman, L., Kosior, E., Favoino, E., Gutberlet, J., Baulch, S., Atreya, M.E., Fischer, D., He, K.K., Petit, M.M., Sumaila, U.R., Neil, E., Bernhofen, M.V., Lawrence, K., Palardy, J.E., 2020, Evaluating scenarios toward zero plastic pollution. Science 369(6510), 1455-1461. http://dx.doi.org/10.1126/science.aba9475.

Li, F., Zimmerman, A.R., Hu, X., Gao, B., 2020, Removal of aqueous Cr(VI) by Zn- and Al-modified hydrochar. Chemosphere 260, 127610-127610. http://dx.doi.org/10.1016/j.chemosphere.2020.127610.

Li, X., Wang, J., You, J., Yu, P., Li, X., Xue, G., Chen, H., Xu, X., van Agtmaal, S., Alvarez, P.J.J., 2019, Hazardous waste dewatering and dry mass reduction through hydrophobic modification by a facile one-pot, alkali-assisted hydrothermal reaction. Water Res. 155, 225-232. http://dx.doi.org/10.1016/j.watres.2019.02.050.

Liu, Y., Zhou, C., Li, F., Liu, H., Yang, J., 2020, Stocks and flows of polyvinyl chloride (PVC) in China: 1980-2050. Resour. Conserv. Recy. 154, 104584. http://dx.doi.org/10.1016/j.resconrec.2019.104584.

Lu, X., Ma, X., Chen, X., Yao, Z., Zhang, C., 2020, Co-hydrothermal carbonization of polyvinyl chloride and corncob for clean solid fuel production. Bioresource. Technol. 301, 122763. http://dx.doi.org/10.1016/j.biortech.2020.122763.

Ma, D., Feng, Q., Chen, B., Cheng, X., Chen, K., Li, J., 2019, Insight into chlorine evolution during hydrothermal carbonization of medical waste model. Journal of Hazardous Materials. http://dx.doi.org/10.1016/j.jhazmat.2019.120847.

Maity, A., Chaudhari, S., Titman, J.J., Polshettiwar, V., 2020, Catalytic nanosponges of acidic aluminosilicates for plastic degradation and CO2 to fuel conversion. Nature Commun. 11(1), 1-12. http://dx.doi.org/10.1038/s41467-020-17711-6.

Matthews, C., Moran, F., Jaiswal, A.K., 2021, A review on European Union's strategy for plastics in a circular economy and its impact on food safety. Journal of Cleaner Production 283. http://dx.doi.org/10.1016/j.jclepro.2020.125263.

Miao, F., Liu, Y., Gao, M., Yu, X., Xiao, P., Wang, M., Wang, S., Wang, X., 2020, Degradation of polyvinyl chloride microplastics via an electro-Fenton-like system with a TiO2/graphite cathode. Journal of Hazardous Materials. http://dx.doi.org/10.1016/j.jhazmat.2020.123023.

Ning, X., Teng, H., Wang, G., Zhang, J., Zhang, N., Huang, C., Wang, C., 2020, Physiochemical, structural and combustion properties of hydrochar obtained by hydrothermal

carbonization of waste polyvinyl chloride. Fuel 270, 117526. http://dx.doi.org/10.1016/j.fuel.2020.117526.

Park, J.-H., Ok, Y.S., Kim, S.-H., Cho, J.-S., Heo, J.-S., Delaune, R.D., Seo, D.-C., 2016, Competitive adsorption of heavy metals onto sesame straw biochar in aqueous solutions. Chemosphere 142, 77-83. http://dx.doi.org/10.1016/j.chemosphere.2015.05.093.

Poerschmann, J., Weiner, B., Woszidlo, S., Koehler, R., Kopinke, F.D., 2015, Hydrothermal carbonization of poly(vinyl chloride). Chemosphere 119, 682-689. http://dx.doi.org/10.1016/j.chemosphere.2014.07.058.

Ramasamy, D.L., Repo, E., Srivastava, V., Sillanpaa, M., 2017, Chemically immobilized and physically adsorbed PAN/acetylacetone modified mesoporous silica for the recovery of rare earth elements from the waste water-comparative and optimization study. Water Res. 114, 264-276. http://dx.doi.org/10.1016/j.watres.2017.02.045.

Rueda-Marquez, J.J., Moreno-Andres, J., Rey, A., Corada-Fernandez, C., Mikola, A., Manzano, M.A., Levchuk, I., 2021, Post-treatment of real municipal wastewater effluents by means of granular activated carbon (GAC) based catalytic processes: A focus on abatement of pharmaceutically active compounds. Water Res. 192, 116833-116833. http://dx.doi.org/10.1016/j.watres.2021.116833.

Sergios, K.P., Evangelos, P.K., Evangelos, P.F., Andreas, A.S., George, E.R., Fotios, K.K., 2010, Metal-carboxylate interactions in metal-alginate complexes studied with FTIR spectroscopy. Carbohyd. Res. http://dx.doi.org/10.1016/j.carres.2009.12.010.

Shen, Y., Yu, S., Ge, S., Chen, X., Ge, X., Chen, M., 2017, Hydrothermal carbonization of medical wastes and lignocellulosic biomass for solid fuel production from lab-scale to pilot-scale. Energy 118, 312-323. http://dx.doi.org/10.1016/j.energy.2016.12.047.

Sheng, K., Zhang, S., Liu, J., E, S., Jin, C., Xu, Z., Zhang, X., 2019, Hydrothermal carbonization of cellulose and xylan into hydrochars and application on glucose isomerization. Journal of Cleaner Production 237, 117831. http://dx.doi.org/10.1016/j.jclepro.2019.117831.

Song, J., Zhang, S., Li, G., Du, Q., Yang, F., 2020, Preparation of montmorillonite modified biochar with various temperatures and their mechanism for Zn ion removal. Journal of Hazardous Materials 391. http://dx.doi.org/10.1016/j.jhazmat.2019.121692.

Tong, S., Shen, J., Jiang, X., Li, J., Sun, X., Xu, Z., Chen, D., 2021, Recycle of Fenton sludge through one-step synthesis of aminated magnetic hydrochar for Pb2+ removal from wastewater. Journal of Hazardous Materials 406. http://dx.doi.org/10.1016/j.jhazmat.2020.124581.

Wang, C., Klamerth, N., Messele, S.A., Singh, A., Belosevic, M., El -Din, M.G., 2016, Comparison of UV/hydrogen peroxide, potassium ferrate(VI), and ozone in oxidizing the organic fraction of oil sands process-affected water (OSPW). Water Res. 100, 476-485. http://dx.doi.org/10.1016/j.watres.2016.05.037.

Wang, J., Guo, X., 2020, Adsorption isotherm models: Classification, physical meaning, application and solving method. Chemosphere 258. http://dx.doi.org/10.1016/j.chemosphere.2020.127279.

Wang, J., Guo, X., 2020, Adsorption kinetic models: Physical meanings, applications, and solving methods. Journal of Hazardous Materials 390.

http://dx.doi.org/10.1016/j.jhazmat.2020.122156.

Wang, X., Zhan, C., Ding, Y., Ding, B., Xu, Y., Liu, S., Dong, H., 2017, Dual-Core Fe2O3@Carbon Structure Derived from Hydrothermal Carbonization of Chitosan as a Highly Efficient Material for Selective Adsorption. Acs Sustain. Chem. Eng. 5(2), 1457-1467. http://dx.doi.org/10.1021/acssuschemeng.6b02034.

Wiedinmyer, C., Yokelson, R.J., Gullett, B.K., 2014, Global Emissions of Trace Gases, Particulate Matter, and Hazardous Air Pollutants from Open Burning of Domestic Waste. Environ. Sci. Technol. 48(16), 9523-9530. http://dx.doi.org/10.1021/es502250z.

Xiao, Y., Hill, J.M., 2020, Solid acid catalysts produced by sulfonation of petroleum coke: Dominant role of aromatic hydrogen. Chemosphere 248. http://dx.doi.org/10.1016/j.chemosphere.2020.125981.

Xiao, Y., Hill, J.M., 2020, Solid acid catalysts produced by sulfonation of petroleum coke: Dominant role of aromatic hydrogen. Chemosphere 248, 125981. http://dx.doi.org/10.1016/j.chemosphere.2020.125981.

Xu, Y., Chen, J., Chen, R., Yu, P., Guo, S., Wang, X., 2019, Adsorption and reduction of chromium(VI) from aqueous solution using polypyrrole/calcium rectorite composite adsorbent. Water Res. 160, 148-157. http://dx.doi.org/10.1016/j.watres.2019.05.055.

Yang, F., Du, Q., Sui, L., Cheng, K., 2021, One-step fabrication of artificial humic acid-functionalized colloid-like magnetic biochar for rapid heavy metal removal. Bioresource. Technol. 328. http://dx.doi.org/10.1016/j.biortech.2021.124825.

Yang, F., Zhang, S., Sun, Y., Du, Q., Song, J., Tsang, D.C.W., 2019, A novel electrochemical modification combined with one-step pyrolysis for preparation of sustainable thorn-like iron-based biochar composites. Bioresource. Technol. 274, 379-385. http://dx.doi.org/10.1016/j.biortech.2018.10.042.

Ye, L., Qi, C., Hong, J., Ma, X., 2017, Life cycle assessment of polyvinyl chloride production and its recyclability in China. Journal of Cleaner Production 142, 2965-2972. http://dx.doi.org/10.1016/j.jclepro.2016.10.171.

Yu, J., Sun, L., Ma, C., Qiao, Y., Yao, H., 2016, Thermal degradation of PVC: A review. Waste Manage. 48, 300-314. http://dx.doi.org/10.1016/j.wasman.2015.11.041.

Zhang, C.Y., Ma, X.Q., Huang, T., Zhou, Y., Tian, Y.L., 2020, Co-hydrothermal carbonization of water hyacinth and polyvinyl chloride: Optimization of process parameters and characterization of hydrochar. Bioresource. Technol. 314, 123676. http://dx.doi.org/10.1016/j.biortech.2020.123676.

649 **Table 1**

650 PFO and PSO model parameters for Cu(II) and Cr(VI) adsorption onto HS-PVC.

Metals	q_{exp}	PFO			PSO		
	(mg/g)	q_1 (mg/g)	R_1^2	k_1 (min^{-1})	q_2 (mg/g)	R_2^2	k_2 (g/(mg·min))
Cu(II)	40.34	38.18	0.86	17.92	40.24	0.95	0.70
Cr(VI)	17.75	15.41	0.88	2.39	16.23	0.94	0.25

651

652
653
654

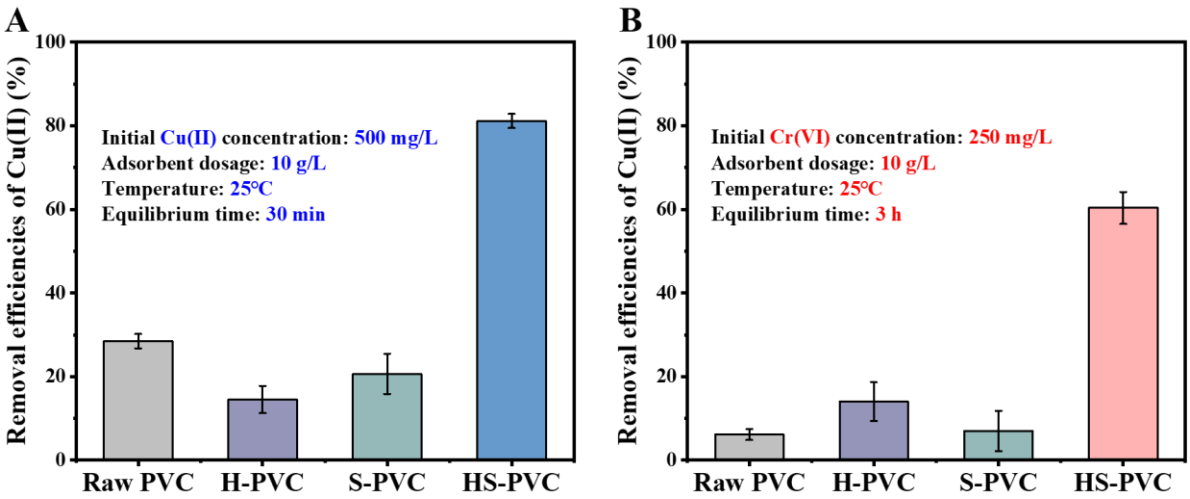

655

656 Fig. 1. Cu(II) and Cr(VI) removal efficiencies using Raw PVC, H-PVC, S-PVC, and

657 HS-PVC after adsorption for 12 hours.

658

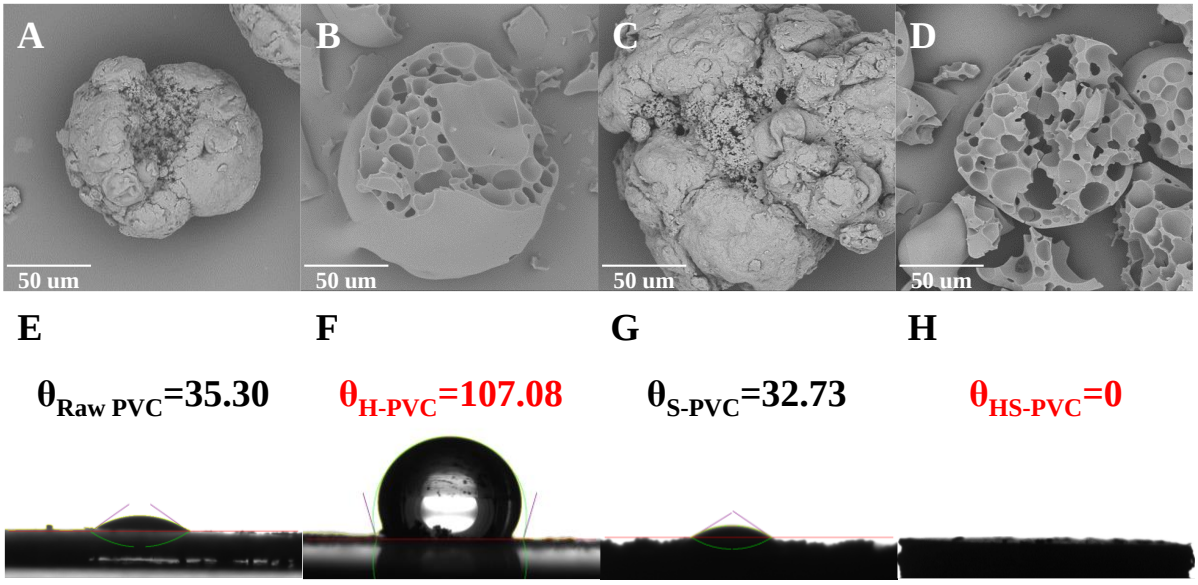

659

660 Fig. 2. Surface properties of PVC derived adsorbents: SEM images of Raw PVC (A), H-PVC

661 (B), S-PVC (C), and HS-PVC (D); contact angle (θ) of Raw PVC (E), H-PVC (F), S-PVC

662 (G), and HS-PVC (I).

663

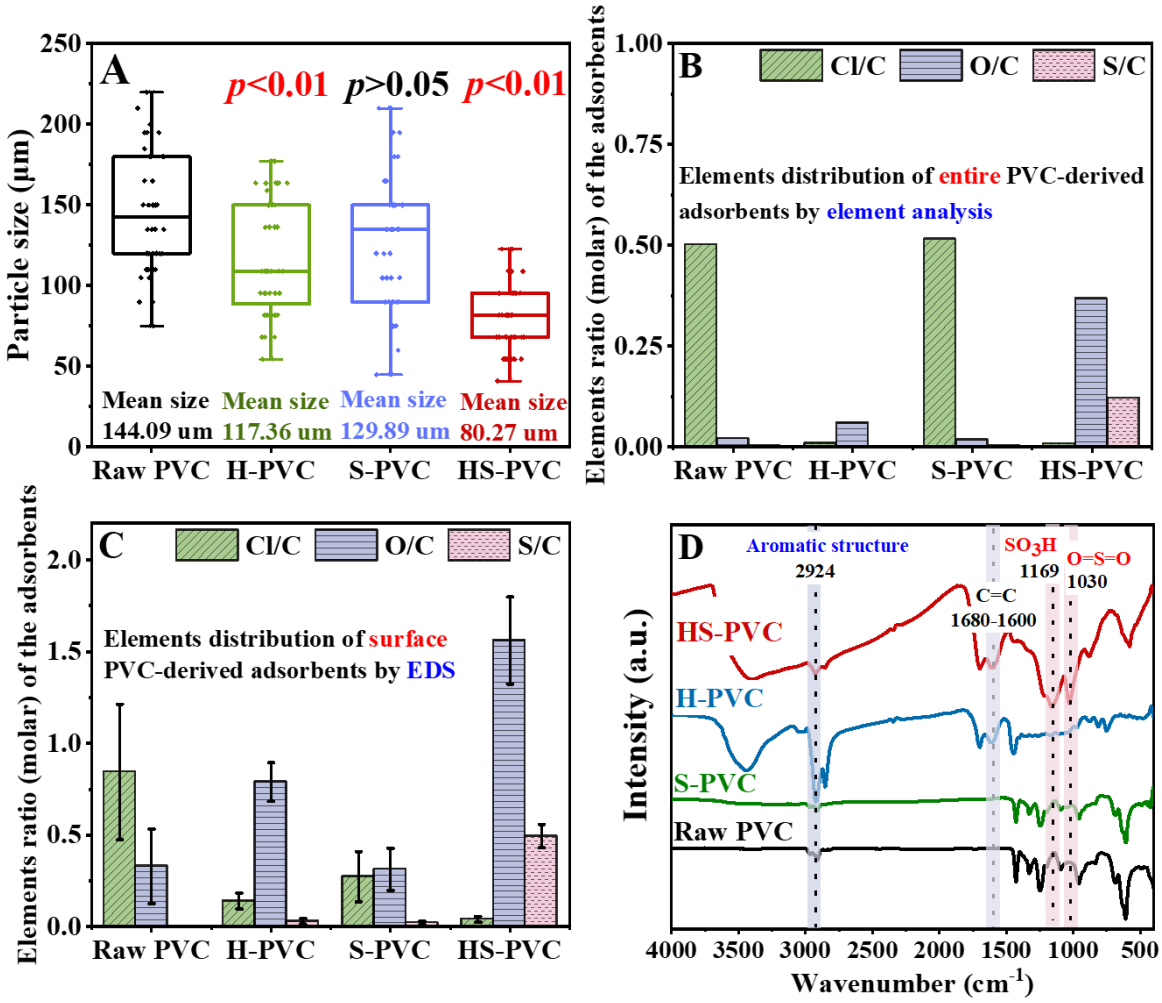

664

665 Fig. 3. Characterization of Raw PVC, H-PVC, S-PVC, and HS-PVC: particle size distribution

666 (A), elemental analysis (B), EDS element mapping (C), and FTIR spectra (D).

667

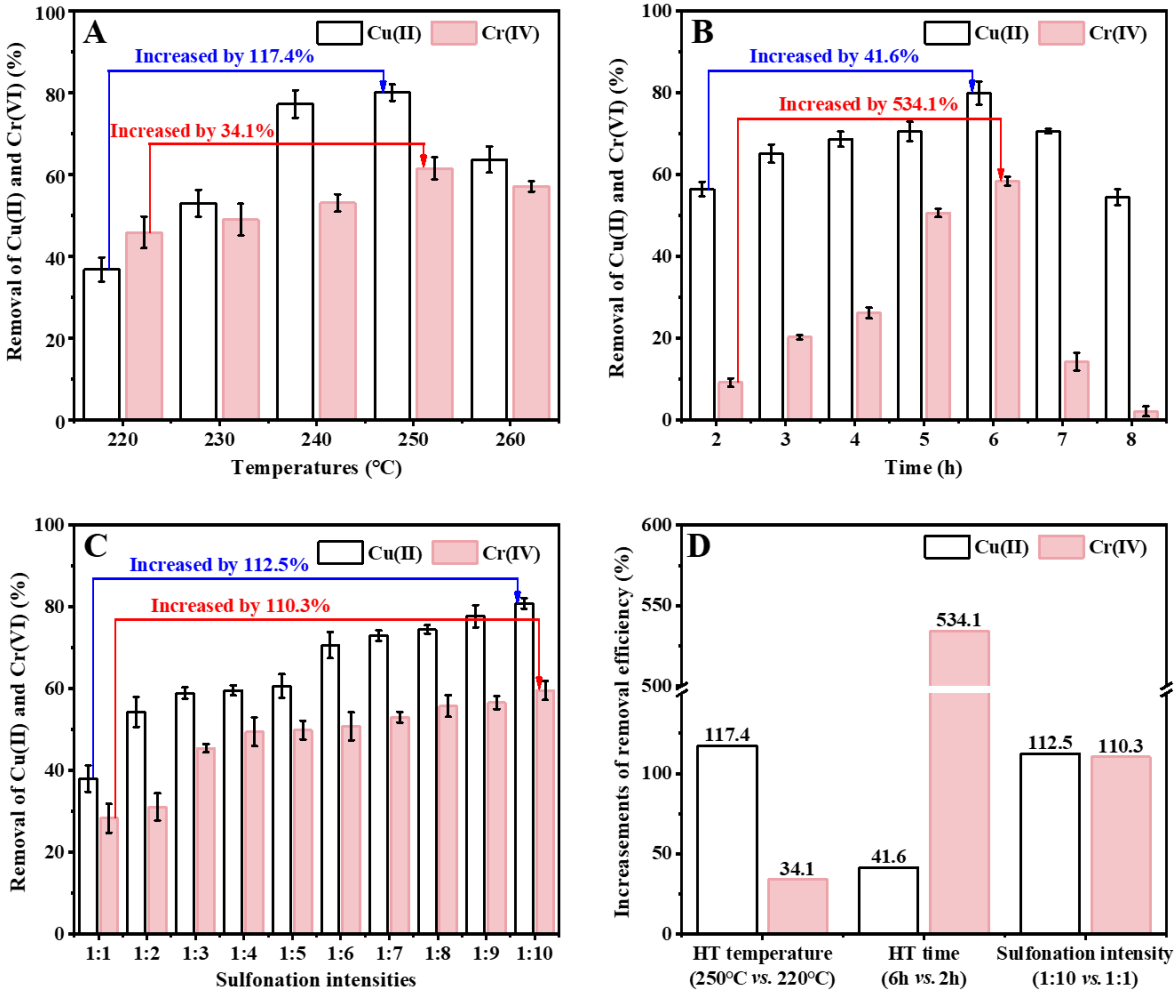

668

669 Fig. 4. Effects of HS-PVC preparation intensities on Cu(II) and Cr(VI) removal: HT

670 temperature (A), HT time (B), sulfonation intensity (C), and comparison of Cu(II) and Cr(VI)

671 removal efficiencies between the optimal and the lowest efficiency (D) (HT temperature: 250 °C

672 *vs.* 220 °C, HT time: 6 h *vs.* 2 h, and sulfonation intensity: 1:10 *vs.* 1:1). The initial

673 concentrations of Cu(II) and Cr(VI) were 500 and 250 mg/L. The adsorbent dose was 10 g/L

674 and the temperature 25 °C.

675

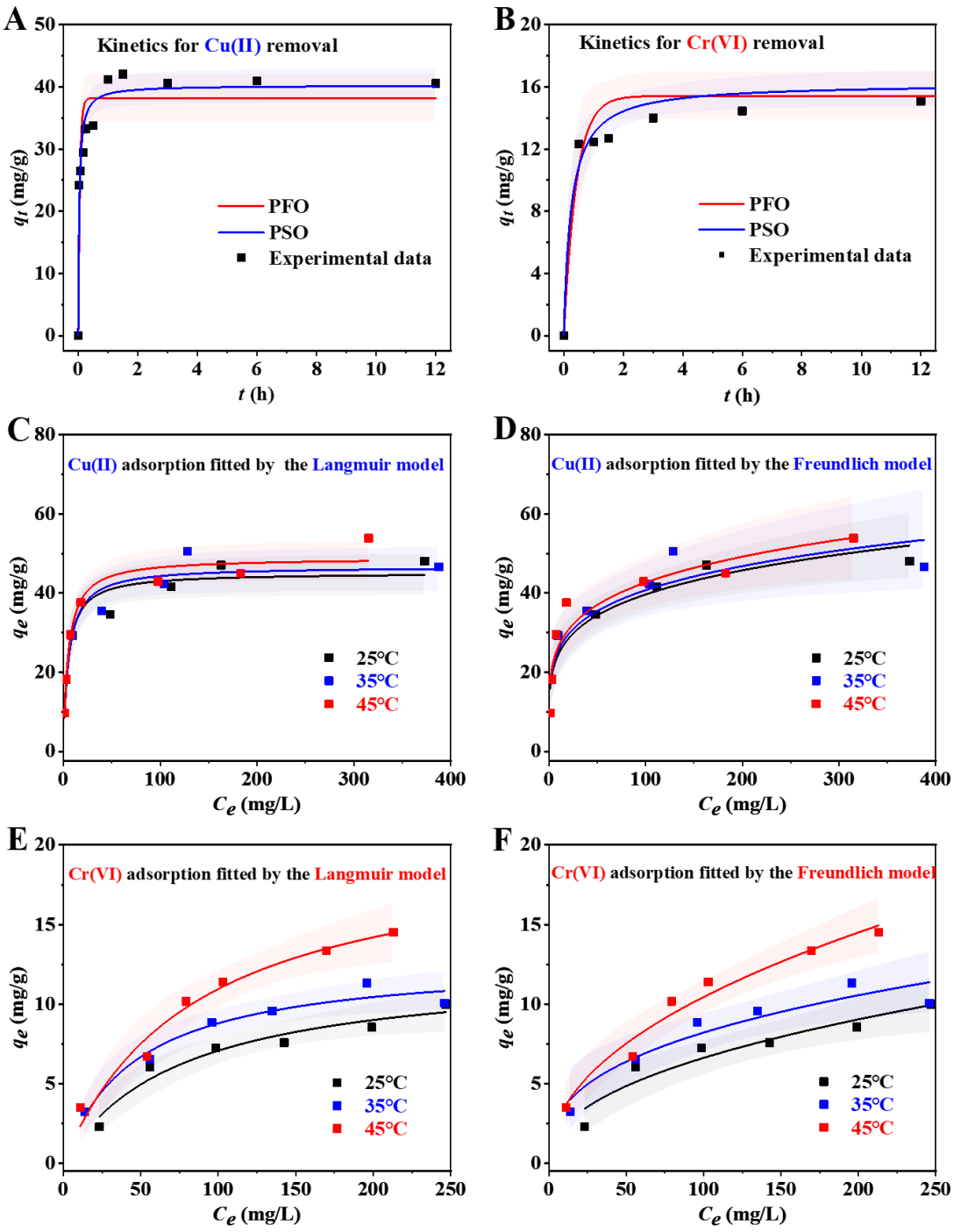

676

677 Fig. 5. Adsorption kinetics of Cu(II) (A) and Cr(VI) (B) onto HS-PVC. Equilibrium
678 isotherms of Cu(II) fitted by the Langmuir (C) and Freundlich models (D) at different
679 temperatures (25, 35, and 45 °C). Equilibrium isotherms of Cr(VI) fitted by the Langmuir (E)
680 and Freundlich models (F) at different temperatures (25, 35, and 45 °C). The colored area
681 covers the 95% confidence intervals.

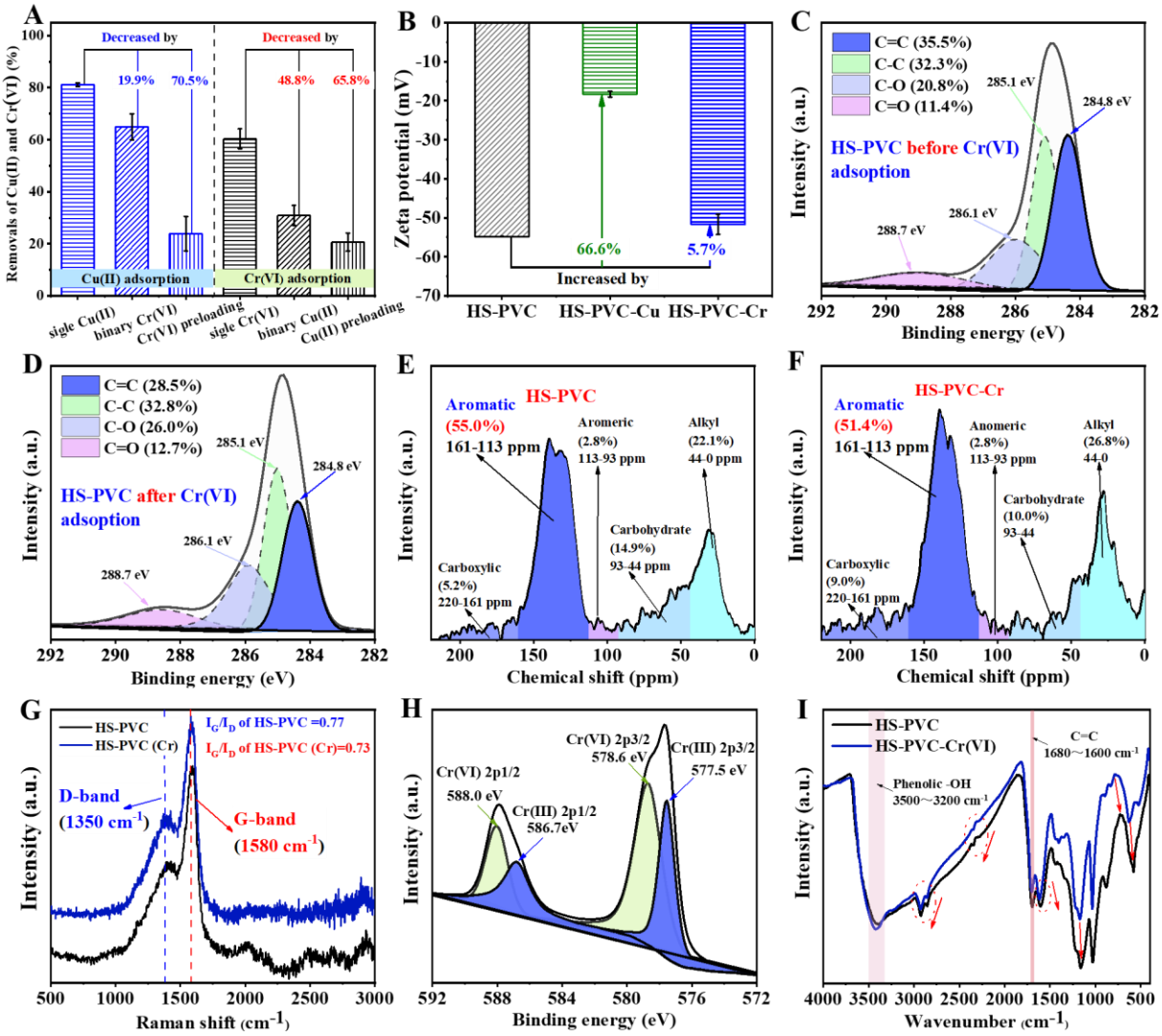

682

683 Fig. 6. Mechanisms for the adsorptions of Cu(II) and Cr(VI) by HS-PVC. Competitive
684 adsorption between Cu(II) and Cr(VI) by HS-PVC (A). Zeta potential of HS-PVC, HS-PVC
685 after the adsorption of Cu(II) (HS-PVC-Cu), and HS-PVC after the adsorption of Cr(VI)
686 (HS-PVC-Cr) (B). C 1s XPS spectra of HS-PVC before the adsorption of Cr(VI) (C) and
687 after the adsorption of Cr(VI) (D). Solid-state ^{13}C NMR of HS-PVC before the adsorption of
688 Cr(VI) (E) and after the adsorption of Cr(VI) (F). Raman spectra of HS-PVC before and after
689 adsorption of Cr(VI) (a higher I_G/I_D ratio indicates a higher degree of graphitization) (G). Cr
690 2p XPS spectra of HS-PVC after the adsorption of Cr(VI) (H). FTIR spectra of HS-PVC
691 before and after the adsorption of Cr(VI) (I).

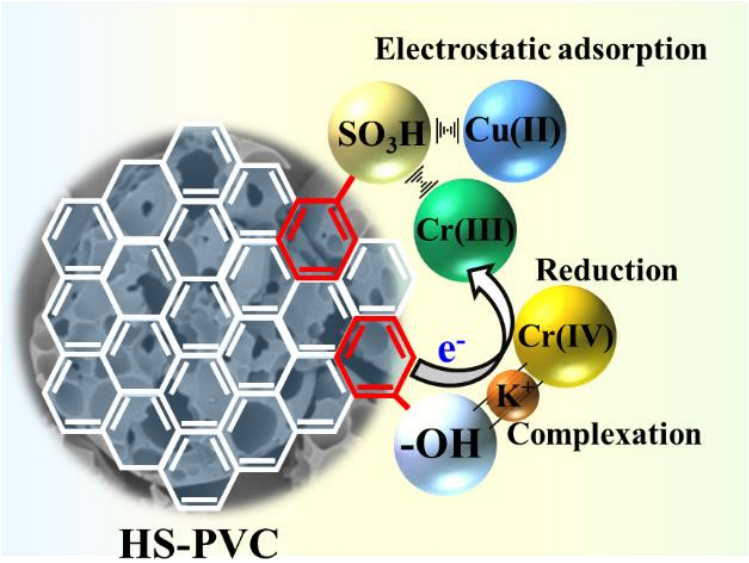

692
693 Fig. 7. Schematic adsorption of Cu(II) and Cr(VI) using HS-PVC
694

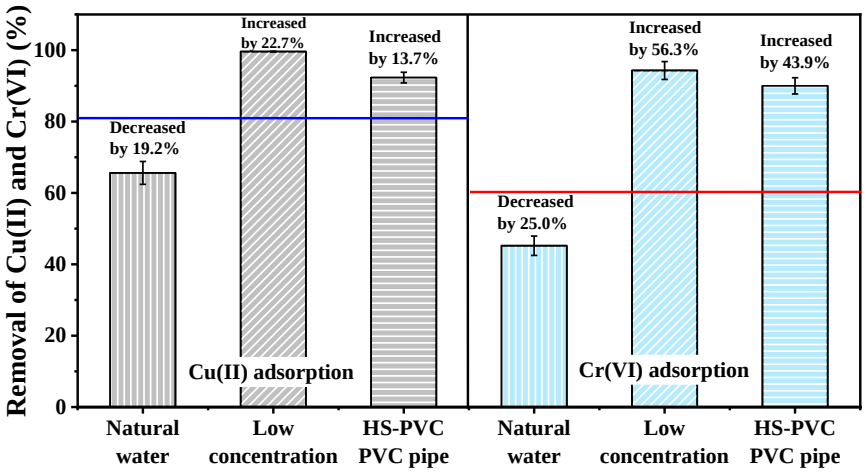

695

696 Fig. 8. Versatility of HS-PVC for Cu(II) and Cr(VI) removal efficiencies. Removal of

697 Cu(II) and Cr(VI) by HS-PVC from natural water, at low concentration (20 mg/L), and by

698 HS-PVC derived from waste PVC pipes (blue and red lines represent the removal efficiency

699 of Cu(II) and Cr(VI) by PVC powder in Fig. 1).

700

701